RSC Applied Polymers

ROYAL SOCIETY OF CHEMISTRY

PAPER

View Article Online
View Journal | View Issue

Cite this: *RSC Appl. Polym.*, 2025, **3**, 1482

Post-synthetic amination of porous hypercrosslinked polymer for the adsorptive removal of bisphenol-A from water

Athira Rajasekharan Sujatha, Saumya Krishnan and Chettiyam Veettil Suneesh *

Microporous organic polymers (MOPs) have garnered significant attention in recent years due to their unique structural and functional properties. Among them, hypercrosslinked polymers (HCPs) are particularly promising for environmental applications, including the removal of organic contaminants from water. In this study, we report the synthesis of a novel HCP, designated as PBFC, constructed *via* Friedel–Crafts knitting alkylation of fluorenone and benzene. Post-synthetic functionalization of PBFC with 1,3-diaminopropane yielded an amine-functionalized polymer, PBFA. The adsorption performance of both polymers was evaluated for the removal of bisphenol-A (BPA) from aqueous solutions. Notably, PBFA exhibited a high adsorption capacity of 130 mg g^{-1}, attributed to the presence of amine groups enhancing interaction with BPA molecules. Adsorption behavior followed the Langmuir isotherm and pseudo-second-order kinetic models, indicating monolayer chemisorption. Thermodynamic analyses revealed negative values of ΔG, ΔH, and ΔS, confirming the spontaneous and exothermic nature of the adsorption process. The dominant adsorption mechanisms were identified as hydrogen bonding, π–π interactions, and hydrophobic interactions. These findings highlight the potential of amine-functionalized HCPs as efficient adsorbents for organic pollutant removal from water.

Received 7th July 2025,
Accepted 24th August 2025

DOI: 10.1039/d5lp00208g

rsc.li/rscapplpolym

1. Introduction

In recent years, the widespread use of synthetic organic compounds has raised serious concerns regarding their environmental and health impacts. Among these, bisphenol-A (BPA), a well-known type-1 endocrine-disrupting chemical (EDC), has become a prominent environmental contaminant due to its extensive application in the production of polycarbonate plastics and epoxy resins. BPA is commonly found in a variety of consumer products, including dental sealants, medical devices, food containers, baby bottles, toys, compact discs, photographic films, pesticides, and other industrial chemicals. The extensive industrial usage and improper disposal of BPA-containing products have led to its persistent release into the environment, ultimately contaminating water resources.[1–4] BPA exposure has been associated with several adverse health effects, including disruptions to brain function, cardiovascular health, behavior, and endocrine activity. Recent studies also link BPA to obesity, breast cancer, allergies, and other chronic conditions.[5–7] In response to these concerns, the European Food Safety Authority (EFSA) has established a tolerable daily intake limit of 0.2 ng kg^{-1} of body weight, underscoring the urgent need to effectively remove BPA from the environment.[8,9]

Numerous strategies have been explored for the removal of organic pollutants from aqueous media, including membrane filtration, biodegradation, coagulation, advanced oxidation processes, and adsorption. Among these, adsorption has emerged as one of the most efficient and cost-effective methods, offering advantages such as operational simplicity, rapid pollutant removal, minimal generation of harmful byproducts, and easy scalability.[2,10,11] Porous organic polymers, particularly microporous frameworks, have recently gained attention as effective adsorbents for water purification. These materials exhibit high thermal and chemical stability, large surface areas, tunable porosity, and diverse functionalization capabilities, making them ideal for pollutant capture *via* non-covalent interactions.[12,13] Within this class, hypercrosslinked polymers (HCPs) stand out due to their superior surface areas, structural rigidity, ease of synthesis *via* the Friedel–Crafts reaction from either natural or synthetic building blocks, and outstanding adsorption properties.[14–18] Furthermore, post-synthetic modification (PSM) of HCPs has proven to be a powerful approach to enhance their adsorption performance. Many organic pollutants, including BPA, contain polar functional groups, and introducing complementary polar functionalities into HCPs can significantly improve their affinity for such contaminants. PSM allows for the tailored incorporation of

Department of Chemistry, University of Kerala, Kariavattom Campus, Thiruvananthapuram-695581, Kerala, India. E-mail: suneesh@keralauniversity.ac.in, suneeshcv@gmail.com

desired functional groups into a pre-formed polymer network, thus optimizing the material for specific environmental applications.[19–22]

In this study, we report the synthesis of an amine-functionalized hypercrosslinked polymer (**PBFA**) *via* the post-synthetic modification of a carbonyl-functionalized precursor (**PBFC**). **PBFC** was synthesized through Friedel–Crafts alkylation of fluorenone and benzene, and subsequently aminated using 1,3-diaminopropane to introduce amine functionalities, yielding **PBFA**. The structural, morphological, and thermal properties of the polymers were characterized in detail. We further evaluated their performance for the adsorption of BPA from aqueous solutions, employing various adsorption isotherms and kinetic models. Additionally, we investigated the possible interaction mechanisms between BPA and **PBFA**. This work demonstrates the potential of post-synthetically modified HCPs as efficient and versatile adsorbents for organic pollutant removal in wastewater treatment applications.

2. Experimental section

2.1 Chemicals

9-Fluorenone (98%) and formaldehyde dimethyl acetal (dimethoxymethane, FDA) (98%) were purchased from Alfa Aesar. 1,2-Dichloroethane (DCE) (99.8%), anhydrous ferric chloride ($FeCl_3$) (99.99%), magnesium sulfate ($MgSO_4{\cdot}7H_2O$) (99%), potassium chloride (KCl) (99%), calcium chloride ($CaCl_2$) (98%) and 1,3-diaminopropane (TDMA) (98%) were obtained from Merk. Benzene (98%), bisphenol-A, sodium borohydride ($NaBH_4$), solvents such as methanol (CH_3OH), *N*,*N*-dimethylformamide (DMF), chloroform ($CHCl_3$), dichloromethane (DCM), tetrahydrofuran (THF) and acetone were obtained from Spectrochem. D-Glucose anhydrous and sodium chloride (NaCl) (99%) were purchased from Nice and Reachem. All the chemicals and solvents were used as received. The adsorption experiments were performed using the distilled water unless otherwise specified.

2.2 Synthesis of hypercrosslinked polymers

2.2.1 Preparation of PBFC. **PBFC** was synthesized *via* a modified Friedel–Crafts alkylation procedure, as outlined in Scheme 1 and based on previously reported method.[23] In a 250 mL round-bottom flask, 9-fluorenone (6.9 g, 38.4 mmol), benzene (3.4 mL, 38.4 mmol), and 1,2-dichloroethane, DCE (78 mL) were added under a nitrogen atmosphere. Anhydrous ferric chloride, $FeCl_3$ (37.4 g, 230.4 mmol) was then introduced and stirred until fully dissolved. Following this, formaldehyde dimethyl acetal, FDA (20 mL, 230.4 mmol) was added dropwise. The reaction mixture was stirred at room temperature for 1 hour and subsequently refluxed at 80 °C for 24 hours. The resulting dark solid was collected by filtration and sequentially washed with methanol, *N*,*N*-dimethylformamide, chloroform, tetrahydrofuran, dichloromethane, and acetone to remove unreacted monomers and reagents. The crude product was further purified *via* Soxhlet extraction with methanol for 24 hours and then dried under vacuum at 120 °C for 24 hours. The final product was obtained as a brown powder in quantitative yield (11.34 g). Characterization data: FTIR, ν = 1715 cm^{-1} (C=O stretch); solid-state ^{13}C NMR (CP/MAS) δ = 200 ppm (carbonyl C), 40 ppm (aliphatic C); elemental analysis: C (56.61%), H, (4.41%).

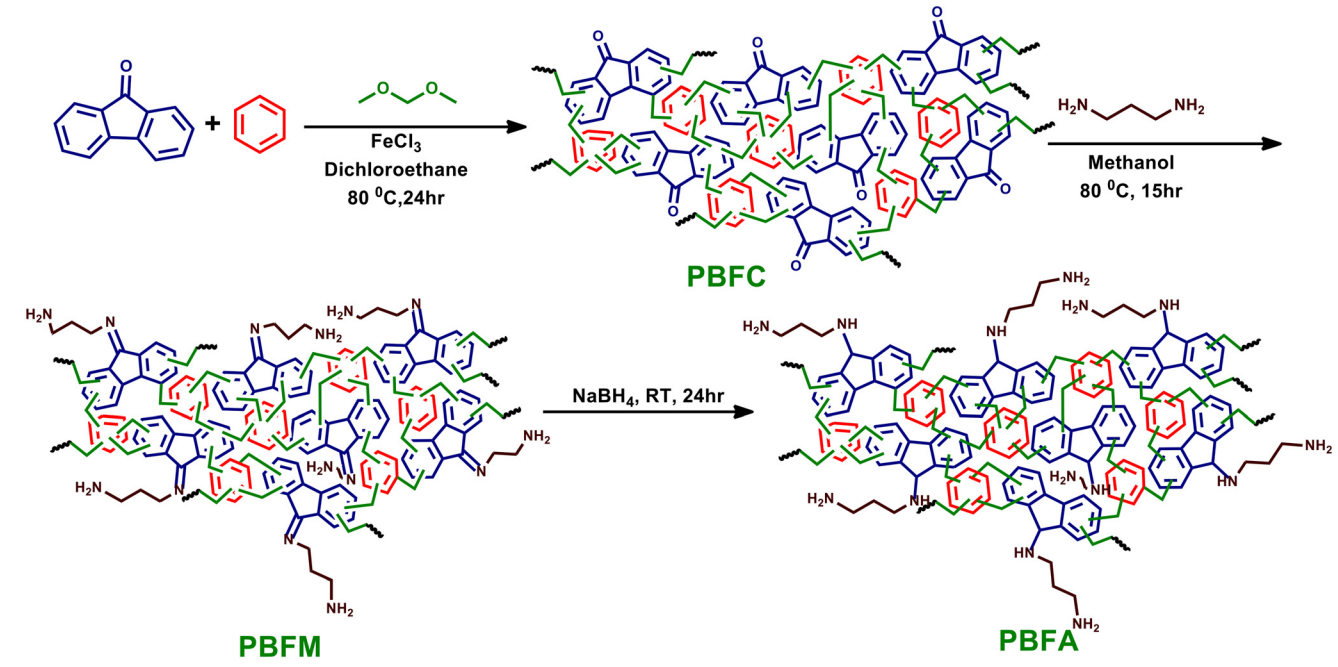

Scheme 1 Synthesis of **PBFC** and **PBFA**.

2.2.2 Preparation of PBFA (post-synthetic modification of PBFC). The post-synthetic modification of PBFC was performed following a slightly modified literature procedure (Scheme 1).[23] In a 250 mL round-bottom flask, 1,3-diaminopropane, TDMA (20 mL, 119.7 mmol), methanol (50 mL), and **PBFC** (5.0 g) were combined. The mixture was refluxed at 80 °C for 15 h under stirring to obtain the imine intermediate, **PBFM**. After cooling to room temperature, reduction of **PBFM** was carried out *in situ* by adding sodium borohydride, $NaBH_4$ (20 g, 528.04 mmol) to the reaction mixture, followed by stirring for an additional 24 h. The resulting solid was collected by filtration, thoroughly washed with methanol, and dried under vacuum at 120 °C for 24 hours. The amine-functionalized polymer, **PBFA**, was obtained as a brown powder in quantitative yield (5.6 g). FTIR ν = 3316, 2981, and 1387 cm^{-1}; solid-state ^{13}C NMR (CP/MAS) δ = 68, 58, and 40 ppm; elemental analysis: C (65.51%), H (5.20%), and N (4.57%).

2.3 Characterization

Fourier-transform infrared (FT-IR) spectra were recorded using an Agilent Technologies Cary 630 FT-IR spectrometer in the range of 650–4000 cm^{-1}. Solid-state ^{13}C nuclear magnetic resonance (^{13}C NMR) spectra were obtained using a 9.4 T JEOL 400 MHz spectrometer. X-ray photoelectron spectroscopy (XPS) analyses were performed with a monochromatic Al Kα X-ray source. Elemental composition was determined using a PerkinElmer 2400 Series II CHNS/O elemental analyzer. Thermogravimetric analysis (TGA) was conducted on a PerkinElmer Simultaneous Thermal Analyzer STA 8000 under a nitrogen atmosphere, with a heating rate of 10 °C min^{-1} from 40 °C to 800 °C. Powder X-ray diffraction (XRD) patterns were collected using a Bruker D8 Advance diffractometer over a 2θ range of 10°–80°. Field-emission scanning electron microscopy (FE-SEM) images were captured using a Nova Nano SEM 450 operated at an accelerating voltage of 10 kV. Nitrogen adsorption–desorption isotherms were measured at 77 K using a Quantachrome Autosorb iQ-MP/XR gas sorption analyzer. Surface area and pore size distribution were calculated using the Brunauer–Emmett–Teller (BET) method and non-local density functional theory (NL-DFT) model *via* ASiQwin software. Prior to analysis, samples were degassed under vacuum at 120 °C for 15 hours. UV–Vis absorption spectra were recorded using a Horiba Duetta fluorescence and absorbance spectrometer.

2.4 Adsorption experiment

Adsorption experiment is shown in Scheme 2. 20 mg of adsorbent was added to 25 mL of BPA solution (20 mg L^{-1}); it was shaken at room temperature and at constant rotations per minute (rpm). The concentration of BPA in the filtrate was measured using a UV-Visible spectrophotometer at 276 nm. The BPA adsorption capacity was calculated as,

$$Q_e = \frac{(C_0 - C_e)}{m} \times V$$

where, V (L) stands for volume of BPA solution, m (g) is the mass of adsorbent, C_0 (mg L^{-1}) and C_e (mg L^{-1}) are initial and equilibrium concentration of BPA. Q_e is expressed in mg g^{-1}. Sorption kinetics and thermodynamics of the BPA adsorption was studied by batch experiments by changing the time intervals and varying the initial concentrations.

2.5 Regeneration experiment

After adsorption the adsorbent was dried under vacuum at 120 °C for 12 hours. To this adsorbent 50 mL of methanol was added and shaken for 12 hours at room temperature, after that the solution was filtered, washed several times with distilled water, and amount of BPA in the filtrate was measured. The cycle was repeated four times for analyzing the reusability of adsorbent.

3. Results and discussion

3.1 Design, synthesis and characterization of PBFC and PBFA

The polymer **PBFC** was synthesized *via* a Friedel–Crafts alkylation reaction, utilizing fluorenone and benzene as the monomers. Formaldehyde dimethyl acetal (FDA) served as the cross-

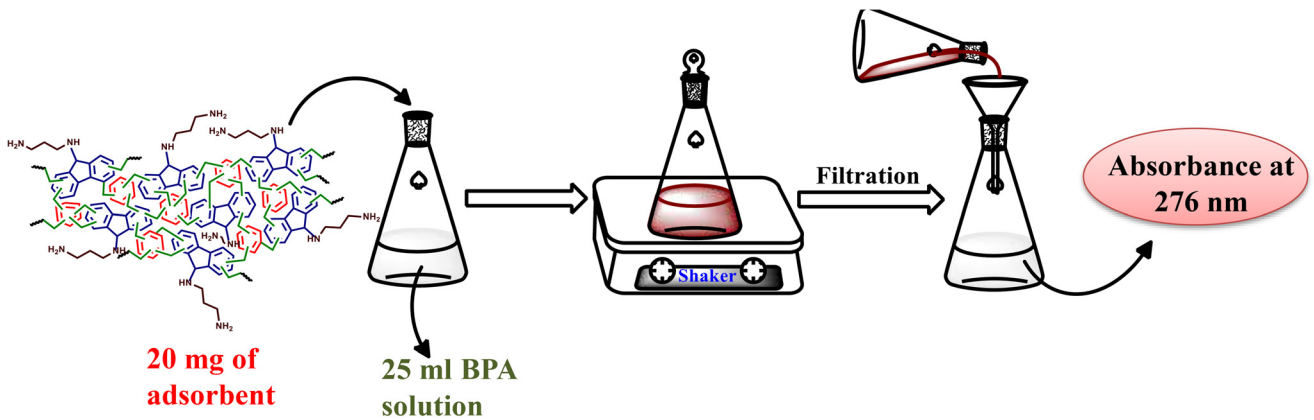

Scheme 2 Procedure for the adsorption experiment.

linking agent, with dichloroethane as the solvent and ferric chloride as the Lewis acid catalyst (Scheme 1). The polymerization was conducted by gradually increasing the temperature from ambient conditions to elevated temperatures to facilitate the formation of a crosslinked network. The resulting polymer was purified through Soxhlet extraction using methanol and subsequently dried under vacuum at 120 °C. Post-synthetic modification of **PBFC** was achieved by reaction with 1,3-diaminopropane (TDMA), yielding the imine intermediate **PBFM**. Subsequent '*in situ*' reduction of **PBFM** with sodium borohydride in methanol afforded the alkyl amine-functionalized polymer **PBFA**.

The FT-IR spectra of **PBFC** and **PBFA** were recorded (Fig. 1). The characteristic peak at 1715 cm^{-1} is attributed to the carbonyl stretching frequency. The –C═O peak vanishes almost completely after the post-synthetic modification, the new peaks appear at 3316 cm^{-1}, 2981 cm^{-1}, and 1387 cm^{-1} corresponds to –NH stretching vibration of the primary amine, secondary amine, and –C–N bond respectively. Additionally, the peaks at 2879 cm^{-1} and 1467 cm^{-1} indicate the –C–H stretching vibration and skeletal vibration of the aromatic ring. One band at 1608 cm^{-1} corresponds to the bending vibration of NH_2 or stretching vibration of –C═C in the aromatic ring.[10,12,23–25] These observations unequivocally confirm the post-synthetic modification of **PBFC** to produce **PBFA**.

The structural transformation from **PBFC** to **PBFA** was further corroborated by solid-state ^{13}C NMR spectroscopy (Fig. 2). The ^{13}C NMR spectrum of PBFC exhibited a prominent resonance at 200 ppm, corresponding to the carbonyl carbon. This signal was absent in the spectrum of **PBFA**, indicating successful post-synthetic modification. In **PBFA**, new peaks emerged at 68 ppm and 58 ppm, consistent with the formation of aliphatic carbon environments introduced during the amine functionalization. A broad set of signals in the range of 110–150 ppm was attributed to aromatic carbons within the polymer backbone. Additionally, a resonance at 40 ppm,

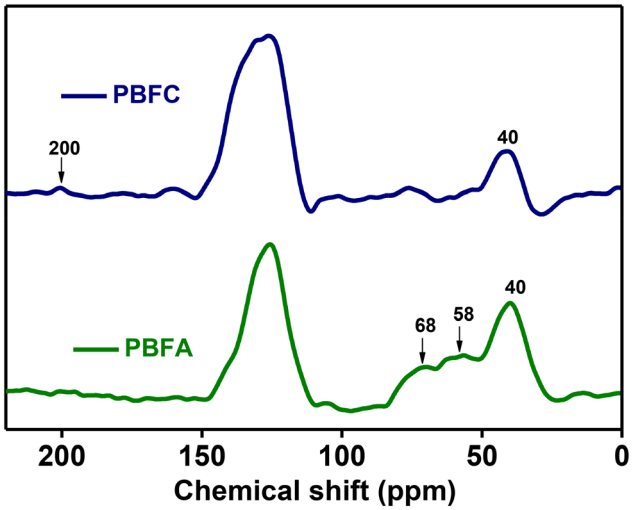

Fig. 2 Solid state ^{13}C NMR spectra of **PBFC** and **PBFA**.

corresponding to methylene (–CH_2–) groups, confirmed the incorporation of formaldehyde dimethyl acetal (FDA) during the polymerization process.[26–28]

Further insights into the chemical composition of the synthesized hypercrosslinked polymers (HCPs) were obtained through X-ray photoelectron spectroscopy (XPS). The XPS survey spectra of **PBFC** and **PBFA** are presented in Fig. 3. The spectrum of **PBFA** displays a distinct N 1s signal, which is absent in **PBFC**, confirming the successful incorporation of nitrogen-containing functionalities following post-synthetic modification. Additionally, an O 1s peak observed in **PBFA** is attributed to the residual carbonyl groups originally present in **PBFC**. High-resolution deconvolution of the C 1s, N 1s, and O 1s core-level spectra (Fig. S1) further supports the structural assignment. The C 1s spectrum reveals peaks at 282 eV, 283 eV, 285.4 eV, and 287 eV, corresponding to C–C, C═C, C–N, and C═O species, respectively. The N 1s spectrum shows a

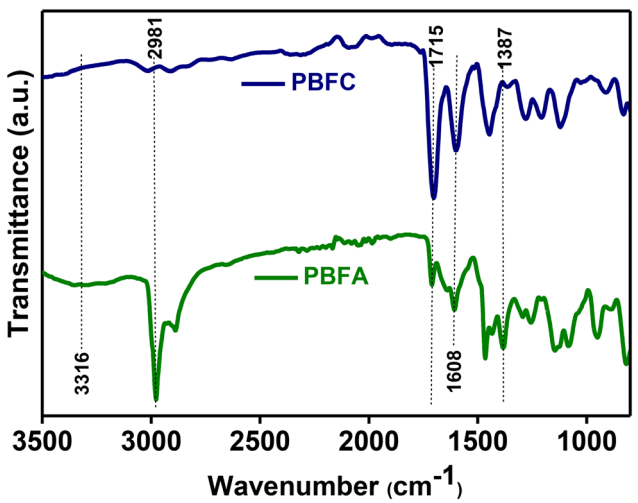

Fig. 1 FT-IR spectra of **PBFC** and **PBFA**.

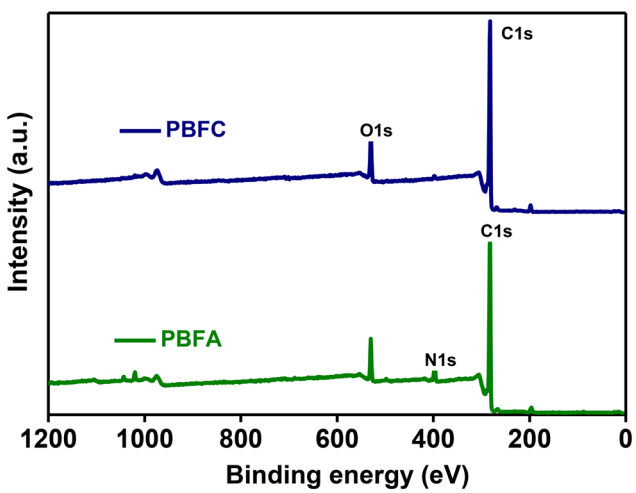

Fig. 3 XPS survey scan spectrum of **PBFC** and **PBFA**.

peak in the range of 396–398 eV, indicative of amine functionalities in **PBFA**. A signal at 530 eV in the O 1s region corresponds to the carbonyl groups present in **PBFC**, consistent with partial retention of unreacted carbonyl functionalities after modification.[26] Elemental analysis (Table S1) revealed an increase in the carbon, hydrogen, and nitrogen content upon conversion of **PBFC** to **PBFA**, further confirming the successful introduction of alkylamine groups on the polymer surface. However, the measured elemental content in both **PBFC** and **PBFA** was slightly lower than the theoretical values, consistent with previous reports.[29] This discrepancy is likely due to additional oxygen content, originating from partially reacted crosslinker or moisture and other atmospheric gases adsorbed under ambient conditions within the microporous structure of the polymer network.[29,30]

The thermal stability of **PBFC** and **PBFA** was evaluated by thermogravimetric (TG) analysis under a nitrogen atmosphere, and the corresponding thermograms are presented in Fig. 4. **PBFC** exhibited thermal stability up to approximately 250 °C, while **PBFA** remained stable up to around 180 °C. The char yields at 800 °C were found to be 34.33 wt% for PBFC and 43.04 wt% for **PBFA**. The increase in char yield following amine functionalization suggests a higher carbon content in **PBFA**. The observed reduction in thermal stability of **PBFA** is likely due to the incorporation of thermally less stable amine groups on the polymer surface.[31] Powder X-ray diffraction (XRD) analysis (Fig. S2) revealed that both **PBFC** and **PBFA** are amorphous, consistent with structural features commonly reported for hypercrosslinked porous polymers. Field-emission scanning electron microscopy (FE-SEM) images (Fig. S3) further confirmed the morphological characteristics of the polymers. Both **PBFC** and **PBFA** exhibited similar surface morphologies, composed of amorphous aggregates with irregular particle shapes. These observations corroborate the amorphous nature indicated by XRD and suggest that the post-synthetic modification does not significantly alter the bulk morphology of the polymer frameworks.

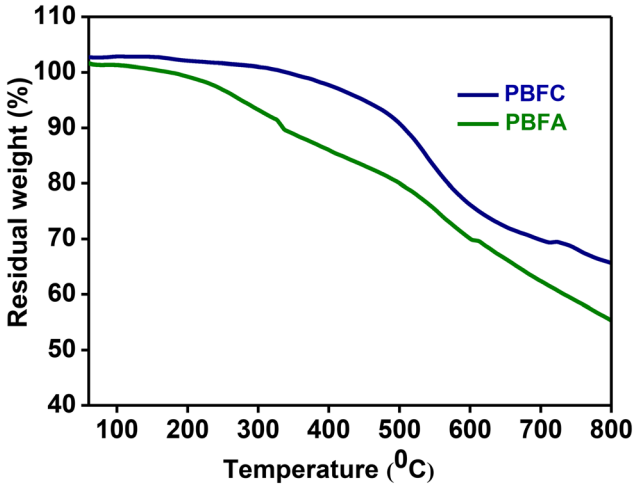

Fig. 4 Thermograms of PBFC and PBFA in the TG analysis.

The surface area and porosity characteristics of the synthesized polymers were investigated using nitrogen adsorption–desorption isotherms at 77 K. The resulting isotherms and pore size distribution curves for **PBFC** and **PBFA** are shown in Fig. 5. Both materials exhibit a combination of type I and type IV isotherms, indicative of the coexistence of microporous and mesoporous structures. A sharp uptake in nitrogen adsorption at low relative pressures (P/P_0 < 0.001) suggests a significant presence of micropores, while the observed hysteresis loop in the desorption branch is attributed to a swelling effect commonly seen in porous organic frameworks.[32,33] The Brunauer–Emmett–Teller (BET) surface areas of **PBFC** and **PBFA** were determined to be 885 $m^2\ g^{-1}$ and 487 $m^2\ g^{-1}$, respectively. The substantial reduction in surface area and microporosity following post-synthetic amination is attributed to the partial blockage of pore channels by the grafted alkylamine groups.[14,23] Pore size distributions were further analyzed using nonlocal density functional theory (NL-DFT), and the derived pore parameters are summarized in Table 1. The results confirm that the majority of the pores in both **PBFC** and **PBFA** fall within the microporous range (<2 nm), while also validating the presence of mesopores, consistent with the mixed isotherm behaviour.

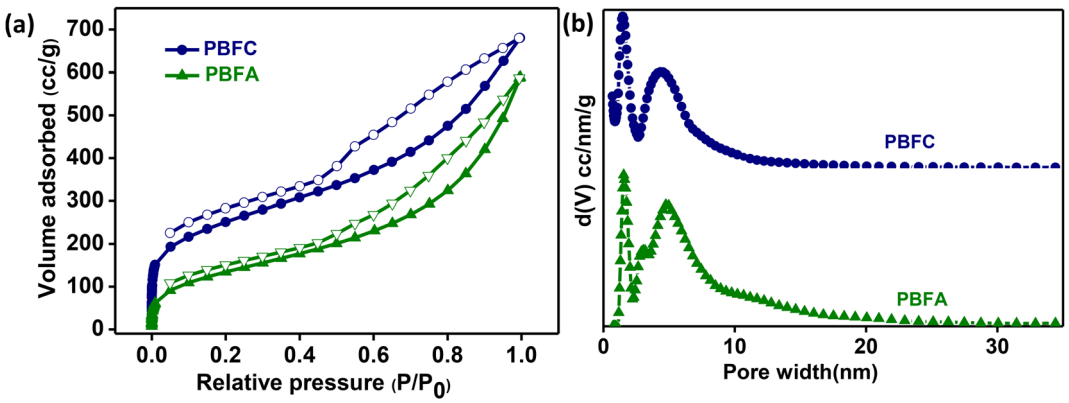

Fig. 5 (a) Nitrogen adsorption–desorption isotherm at 77 K and (b) pore size distribution curve of PBFC and PBFA.

Table 1 Pore parameters of **PBFC** and **PBFA**

Samples	S_{BET} ($m^2\ g^{-1}$)	$S_{Langmuir}$ ($m^2\ g^{-1}$)	V_{total} ($cm^3\ g^{-1}$)	V_{micro} ($cm^3\ g^{-1}$)	Pore size (nm)
PBFC	885	1103	0.965	0.345	1.33, 4.10
PBFA	487	655	0.762	0.221	1.73, 4.40

3.2 Adsorption studies of BPA

3.2.1 Comparison of adsorption capacities of BPA onto PBFC and PBFA. Batch adsorption experiments were performed to evaluate the adsorption capacities of **PBFC** and **PBFA** for bisphenol-A (BPA) at 298 K, focusing on the effects of solution pH and initial BPA concentration. pH is a critical factor influencing the adsorption behaviour of BPA due to its impact on both the adsorbent surface and the ionization state of the adsorbate. To assess this effect, 20 mg of each adsorbent (**PBFC** or **PBFA**) was added to 25 mL of BPA solution with pH values ranging from 2 to 9. As shown in Fig. 6a, **PBFA** exhibited relatively consistent adsorption capacity across the acidic to near-neutral pH range, with a slight increase from pH 2 to 6.5 and a marginal decrease thereafter. In contrast, **PBFC** displayed a significant pH-dependent increase in adsorption capacity from pH 2 to 7, beyond which the adsorption remained nearly constant. This variation is attributed to the nature of the functional groups in each polymer: **PBFA** contains $-NH_2$ groups, while **PBFC** features carbonyl (C═O) functionalities in its polymer skeleton. At lower pH, the $-NH_2$ groups in **PBFA** are protonated, but still capable of forming hydrogen bonds with BPA. Meanwhile, the protonated environment suppresses the electron-donating ability of the carbonyl oxygen in **PBFC**, thereby reducing its interaction with BPA. As the pH increases toward neutrality, deprotonation of functional sites on both **PBFA** and **PBFC** enhances the interaction with BPA through hydrogen bonding and π–π interactions. BPA exists predominantly in its neutral molecular form below its pK_a (~9.6), making it more amenable to hydrophobic and non-covalent interactions.[5,31,32,34–36] The plateau observed in **PBFC** adsorption capacity beyond pH 7 can be explained by the saturation of available adsorption sites and the stabilization of intermolecular interactions between BPA and the carbonyl functionalities of the polymer. The enhanced capacity of **PBFA** is primarily driven by the synergistic effects of hydrogen bonding, π–π interactions, and the presence of electron-rich nitrogen functionalities introduced during amination.

To further evaluate the adsorption behaviour, the effect of initial BPA concentration on the adsorption capacity of **PBFC** and **PBFA** was studied at 298 K (Fig. 6b). The results show that **PBFA** consistently exhibits a higher BPA adsorption capacity than **PBFC** across all concentrations, despite having a lower specific surface area. This enhanced performance is attributed to the presence of alkylamine functional groups on the surface of **PBFA**, which likely provide additional active sites and promote stronger interactions with BPA molecules. The superior adsorption capacity of **PBFA**, even under conditions of lower surface area, highlights the significant role of surface chemistry, particularly amine functionalities in enhancing adsorption efficiency. These initial findings underscore the potential of **PBFA** as a promising adsorbent for BPA removal from aqueous environments, warranting further studies under various affecting factors to assess its practical applicability in water purification systems.

3.2.2 BPA adsorption studies of PBFA

3.2.2.1 Adsorption kinetics (effect of contact time on adsorption). Kinetic studies of BPA adsorption onto **PBFA** were conducted at 298 K using varying initial BPA concentrations (20, 60, 100, and 200 mg L^{-1}), as shown in Fig. 7. The results demonstrate that the adsorption capacity increases with rising initial BPA concentration. A rapid adsorption rate was observed during the initial stages of the process, followed by a gradual slowdown as equilibrium was approached around 150 minutes. This behavior can be attributed to the abundance of available active sites on the **PBFA** surface at the beginning, which become progressively saturated over time, reducing the rate of adsorption.[37]

To better understand the adsorption kinetics and underlying mechanism, the experimental data were analyzed using two common kinetic models: the pseudo-first-order and

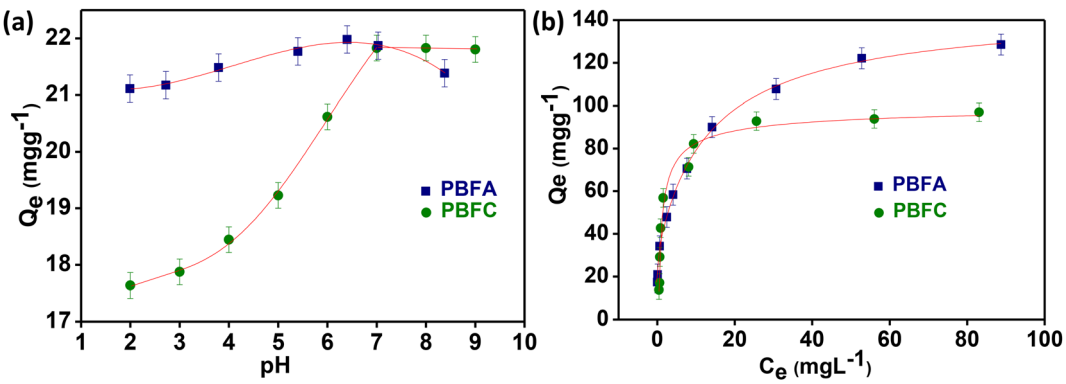

Fig. 6 (a) Effect of pH and (b) effect of initial concentration of BPA adsorption onto **PBFC** and **PBFA** at 298 K (20 mg adsorbent, 25 mL of 20 mg L^{-1} BPA).

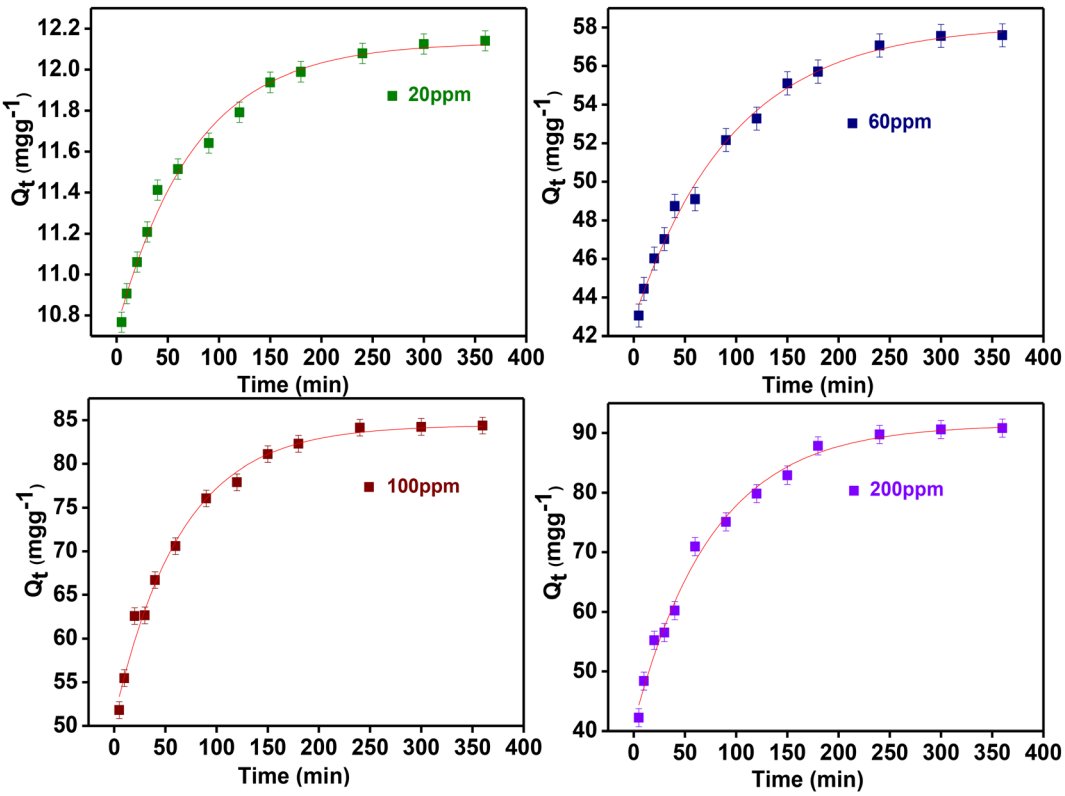

Fig. 7 Effect of contact time on adsorption at various concentrations of BPA solution (20 mg adsorbent, 25 mL BPA solution, 298 K).

pseudo-second-order models. The linearized equations for both models are provided in eqn (a) and (b)[38,39]

$$\ln(Q_e - Q_t) = -k_1 t + \ln Q_e \quad \text{(a)}$$

$$\frac{t}{Q_t} = \frac{t}{Q_e} + \frac{1}{k_2 Q_e^2} \quad \text{(b)}$$

where, Q_e (mg g^{-1}) and Q_t (mg g^{-1}) are the adsorption capacity of BPA on **PBFA** at equilibrium and time t (min). The parameters k_1 and k_2 represent the pseudo-first-order and pseudo-second-order rate constants. The corresponding kinetic parameters are summarized in Table 2. The results indicate that the pseudo-second-order model provides a better fit to the experimental data, as evidenced by higher correlation coefficient (R^2) values approaching unity. The model fitting plots are shown in Fig. S5. The superior fit of the pseudo-second-order model suggests that the BPA adsorption process on **PBFA** is governed primarily by chemisorption, involving valence forces through the sharing or exchange of electrons between the adsorbent and BPA molecules.[6,35,40,41] These findings further support the suitability of **PBFA** as an effective adsorbent for the removal of BPA from aqueous solutions.

3.2.2.2 Adsorption isotherm (effect of initial concentration and temperature). Adsorption isotherms provide critical insights into the adsorption capacity of an adsorbent and the nature of interactions between the adsorbent and the adsorbate. In this study, equilibrium adsorption isotherms for BPA on **PBFA** were obtained at three different temperatures: 298 K, 313 K, and 323 K (Fig. 7). The results reveal that the adsorption capacity of **PBFA** decreases with increasing temperature, indicating that the adsorption process is exothermic in nature.[42–44] The maximum adsorption capacity observed was 130 mg g^{-1} at 298 K. Additionally, adsorption capacity increased with rising initial BPA concentrations, eventually reaching equilibrium at

Table 2 Pseudo-first and pseudo-second order kinetic parameters for BPA adsorption

		Pseudo-first-order			Pseudo-second-order		
C_e (mg L^{-1})	Q_e (mg g^{-1}) (expt)	Q_e (mg g^{-1})	k_1 (min^{-1})	R^2	Q_e (mg g^{-1})	k_2 (g mg^{-1} min^{-1})	R^2
20	12.112	2.039	0.0197	0.9015	12.345	0.0308	0.9999
60	57.634	18.988	0.0142	0.8543	58.513	0.0023	0.9991
100	84.090	26.284	0.0019	0.0699	86.505	0.0012	0.9992
200	90.469	39.165	0.0042	0.1116	94.876	0.0006	0.9976

higher concentrations, reflecting saturation of available adsorption sites.

To further analyze the adsorption behavior, the equilibrium data were fitted using both Langmuir and Freundlich isotherm models. The linear forms of the equations are,

$$\frac{C_e}{Q_e} = \frac{1}{Q_m K_L} + \frac{C_e}{Q_m} \quad (c)$$

$$\ln Q_e = \ln K_F + \frac{1}{n} \ln C_e \quad (d)$$

where, Ce (mg L^{-1}) is the concentration of BPA at equilibrium, Q_m (mg g^{-1}) is the maximum adsorption capacity, K_L (L mg^{-1}) is the Langmuir constant, K_F (L mg^{-1}) and n is the Freundlich constant.[44] The model parameters and corresponding fitting results are presented in Table 3 and Fig. 8. Among the two, the Langmuir model exhibited superior correlation with the experimental data ($R^2 > 0.97$), suggesting that BPA adsorption on **PBFA** occurs *via* monolayer coverage on a homogeneous surface, consistent with a chemisorption mechanism.[2,7,45] Furthermore, the maximum monolayer adsorption capacity (Q_m) and Langmuir constant (K_L) decreased with increasing temperature, reaffirming the preference for adsorption at lower temperatures.[42,43]

The favorability of the adsorption process was further evaluated using the dimensionless separation factor (K_R), derived from the Langmuir isotherm. This parameter indicates the nature of adsorption: favorable ($0 < K_R < 1$), linear ($K_R = 1$), unfavorable ($K_R > 1$), or irreversible ($K_R = 0$).[46] K_R values calculated at all studied temperatures are summarized in Table S2. All values fell within the favorable range, confirming the suitability of **PBFA** for BPA adsorption across the tested temperatures. Notably, the lowest K_R

Table 3 Langmuir and Freundlich parameters for adsorption isotherm model

		Langmuir			Freundlich		
T (K)	Q_e (mg g^{-1}) (expt)	Q_m (mg g^{-1})	K_L (L mg^{-1})	R^2	n_F	K_F (L mg^{-1})	R^2
298	130.0	131.06	0.273	0.9916	4.133	43.737	0.9798
313	109.2	115.34	0.164	0.9890	2.419	21.542	0.8919
323	95.0	108.11	0.136	0.9893	3.129	25.262	0.9733

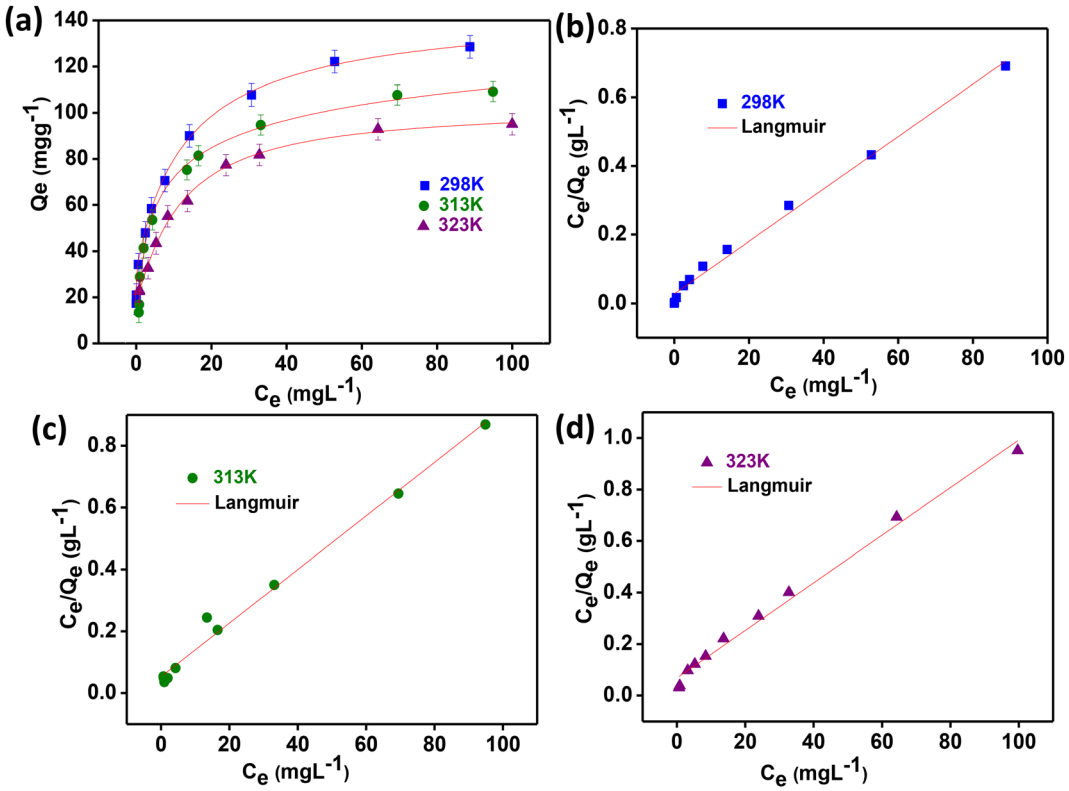

Fig. 8 (a) Effect of temperature on BPA adsorption, (b), (c), and (d) Langmuir fitting curves (20 mg adsorbent, 25 mL BPA solution).

value was observed at 298 K, indicating that the adsorption process is most favorable at this temperature.

$$K_R = \frac{1}{1 + K_L C_0} \quad \text{(e)}$$

where C_0 (mg L^{-1}) is the initial concentration of BPA.

3.2.2.3 Thermodynamic studies. Thermodynamic parameters provide valuable insight into the nature and feasibility of the adsorption process. To evaluate the thermodynamics of BPA adsorption on **PBFA**, batch experiments were performed at three different temperatures: 298 K, 313 K, and 323 K. The standard Gibbs free energy change ($\Delta G°$), enthalpy change ($\Delta H°$), and entropy change ($\Delta S°$) were calculated using the following eqn (f) and (g) and are summarized in Table 4.

$$\Delta G = -RT \ln K_L \quad \text{(f)}$$

$$\ln K_L = -\frac{\Delta H}{RT} + \frac{\Delta S}{R} \quad \text{(g)}$$

K_L is the Langmuir constant in L g^{-1}, R is the gas constant (8.314 J K^{-1} mol^{-1}), T is the temperature in Kelvin, ΔH (kJ mol^{-1}) and ΔS (kJ K^{-1} mol^{-1}) were calculated from slope and intercept of $\ln K_L$ *versus* $1/T$ plot (Fig. S7).[42]

The $\Delta G°$ values for all tested temperatures are negative, confirming that the adsorption of BPA onto **PBFA** is a spontaneous process. Moreover, the magnitude of $\Delta G°$ slightly decreases with increasing temperature, suggesting that spontaneity diminishes at higher temperatures, consistent with an exothermic adsorption mechanism. The negative value of $\Delta H°$ (−22.53 kJ mol^{-1}) further supports the exothermic nature of the adsorption process and falls within the range typically associated with chemisorption. The entropy change ($\Delta S°$) is also negative (−29.13 J mol^{-1} K^{-1}), indicating a decrease in randomness at the solid–solution interface during adsorption. This suggests a more ordered arrangement of BPA molecules on the **PBFA** surface, which is characteristic of specific interactions such as hydrogen bonding and π–π stacking, commonly involved in chemisorption.[6,35,36,42,43] Overall, the thermodynamic analysis confirms that BPA adsorption onto **PBFA** is spontaneous, exothermic, and likely governed by chemisorption mechanisms.

3.2.2.4 Regeneration studies of BPA adsorption. The regeneration and reusability of **PBFA** were evaluated to assess its potential for repeated BPA adsorption cycles. After each adsorption cycle, the BPA-loaded **PBFA** was treated with methanol and stirred in a water bath shaker at 298 K for 12 hours. Methanol was chosen as the desorption solvent due to the high solubility of BPA, which facilitates the disruption of interactions between BPA and the **PBFA** surface. The regenerated adsorbent was subsequently filtered, thoroughly washed with deionized water, and dried under vacuum at 120 °C for 12 hours before reuse. The adsorption capacities of **PBFA** over four successive regeneration cycles are shown in Fig. 9. The BPA removal efficiency remained high over multiple cycles, showing only a slight decrease from 96% in the first cycle to 90% after four cycles. This high level of performance highlights the excellent stability and regenerability of **PBFA**, indicating its potential as a sustainable and reusable adsorbent for BPA removal in water treatment applications.

3.2.3 BPA adsorption studies of PBFA in simulated wastewater. To assess the practical applicability of **PBFA** for BPA removal, a stock solution of simulated wastewater was prepared containing 500 mg L^{-1} BPA, 125 mg L^{-1} $MgSO_4 \cdot 7H_2O$, 150 mg L^{-1} NaCl, 500 mg L^{-1} $CaCl_2$, 12.5 mg L^{-1} KCl and 250 mg L^{-1} D-glucose.[47] Simulated wastewater samples with varying BPA concentrations were subsequently prepared, and the corresponding adsorption capacities of **PBFA** were evaluated (Fig. 10). **PBFA** exhibited a maximum BPA adsorption capacity of 127 mg g^{-1} in simulated wastewater, closely matching its performance in distilled water (130 mg g^{-1}). These results demonstrate that **PBFA** retains excellent adsorption efficiency in complex aqueous environments, underscoring its potential for real-world wastewater treatment applications.

3.2.4 Mechanism of BPA adsorption on PBFA. The adsorption mechanism of BPA onto **PBFA** can be attributed to multiple interactions, including pore-filling, hydrophobic interactions, π–π stacking, and hydrogen bonding. Given that the average molecular size of BPA is 1.25 nm and that the pore diameter of **PBFA** is approximately 1.73 nm, BPA molecules can easily access and diffuse into the pores of **PBFA**, supporting a pore-filling mechanism that enhances adsorption capacity.[48] The pH of the adsorption system was maintained at 6.5, which is below the pK_a of BPA. Under these conditions, BPA predominantly exists in its neutral molecular form, favouring interactions with the aromatic and functional moieties of the

Table 4 Thermodynamic parameters for BPA adsorption

T (K)	$(1/T) \times 10^{-3}$ K^{-1}	$\ln K_L$	ΔG (kJ mol^{-1})	ΔH (kJ mol^{-1})	ΔS (J mol^{-1} K^{-1})
298	3.355	5.608	−13.896	−22.534	−29.129
313	3.194	5.103	−13.279		
323	3.095	4.916	−13.202		

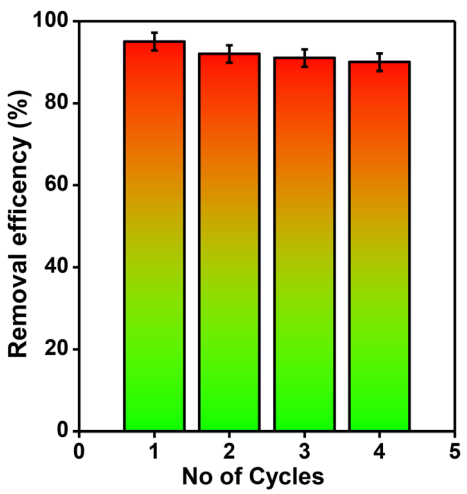

Fig. 9 Regeneration studies of BPA adsorption.

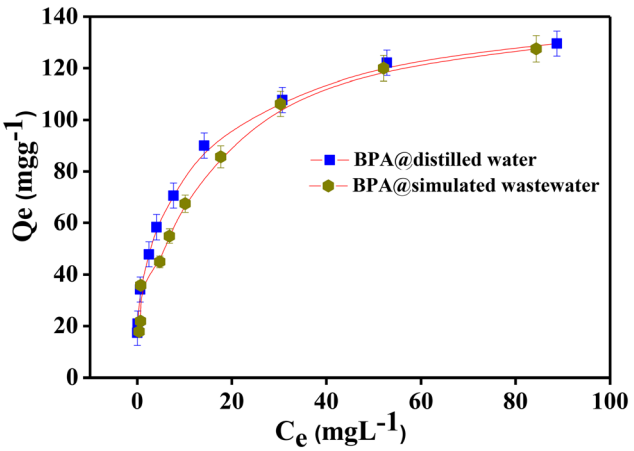

Fig. 10 Comparison of BPA adsorption studies of **PBFA** in simulated wastewater and distilled water (20 mg adsorbent, 25 mL BPA solution).

adsorbent, **PBFA**.[6,32] This observation suggests that electrostatic interactions are negligible and do not play a significant role in the adsorption process.

The hydrophobic nature of **PBFA**, derived from its aromatic-rich hypercrosslinked polymeric structure, also plays an important role. BPA, being a hydrophobic aromatic compound, can interact favourably with the **PBFA** surface *via* hydrophobic interactions, thereby facilitating adsorption.[6,32,48–50] Additionally, **PBFA** is a π-electron-rich material capable of forming π–π interactions with the phenyl rings of BPA (Scheme 3).[38] This interaction was investigated through XPS analysis of the **PBFA** before and after BPA adsorption (**BPA@PBFA**), as shown in Fig. 11.[10,50] The deconvoluted C 1s spectra revealed binding energy shifts in the C═C, C–C, and C═N components from 283.2, 282.2, and 285.4 eV to 282.6, 281.9, and 284.0 eV, respectively, after BPA adsorption. These shifts confirm the occurrence of π–π interactions between BPA and the **PBFA** framework.

Hydrogen bonding interactions also contribute to the overall adsorption mechanism, owing to the high nitrogen content in **PBFA**. This was confirmed by comparing the FT-IR spectra of pristine **PBFA** and **BPA@PBFA** (Fig. 12). After adsorption, the –NH stretching peak shifted from 2981 cm^{-1}

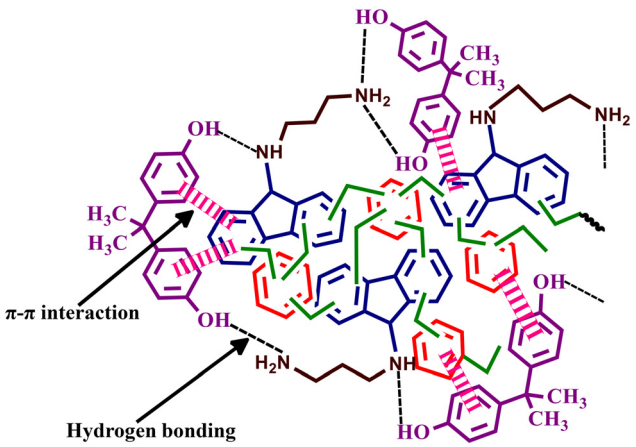

Scheme 3 Schematic representation of BPA adsorption mechanism on **PBFA**.

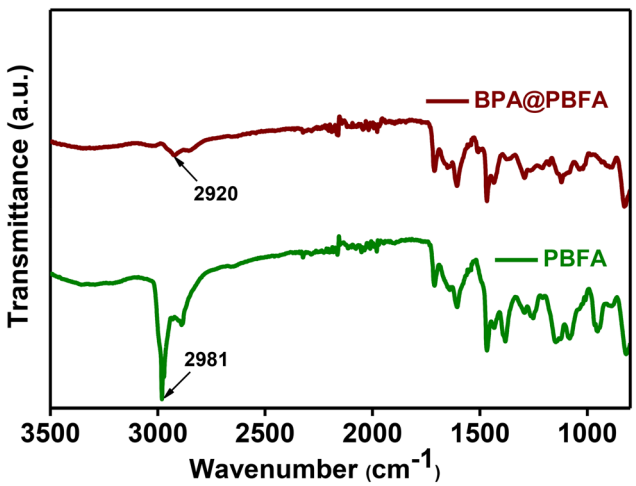

Fig. 12 FT-IR spectrum of **PBFA** and (**BPA@PBFA**).

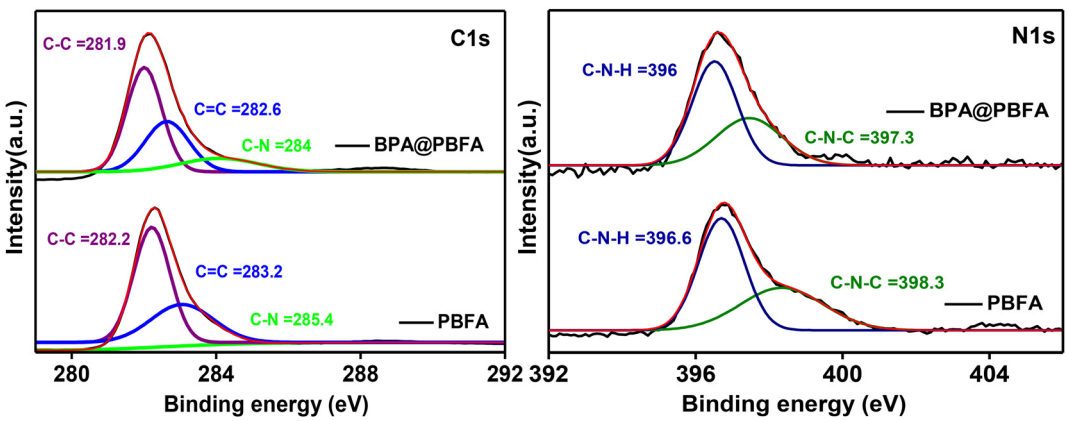

Fig. 11 Deconvoluted C 1s and N 1s spectrum of **PBFA** and **BPA@PBFA**.

to 2920 cm^{-1}, accompanied by a reduction in intensity. Additionally, the –C–N bond intensity also reduces, indicating the formation of hydrogen bonds between the –NH groups of **PBFA** and the –OH groups of BPA (Scheme 3).[14] The N 1s XPS spectra of **BPA@PBFA** also showed a shift toward lower binding energy, further supporting the role of hydrogen bonding.[10] In short, the adsorption of BPA onto **PBFA** is predominantly governed by hydrophobic interactions, π–π stacking, and hydrogen bonding. The synergistic contribution of these mechanisms facilitates the efficient removal of BPA from aqueous media.

The comparative analysis of various adsorbents for BPA removal, as summarized in Table S3, highlights the superior performance of the newly developed **PBFA** material. The superior adsorption capacity, rapid adsorption kinetics, high surface area, and operation at near-neutral pH underscore the efficiency of **PBFA**, which outperforms most of the previously reported materials. **PBFA** exhibited a high adsorption capacity of 130 mg g^{-1}, surpassing most reported adsorbents such as carbon nanotubes, β-CDP and β-cyclodextrin grafted cellulose beads, and was comparable to MSNCTAB and COF-2.[5,31,50,51] The equilibrium was achieved within 150 min, which is faster than several high-capacity adsorbents requiring extended contact times but slower than rapid adsorbents such as β-CDP and BDE-T-CDP(B).[51,52] The optimal adsorption occurred at pH 6.5, which is close to neutral and advantageous for practical wastewater treatment by minimizing pH adjustment compared to adsorbents operating under strongly acidic or alkaline conditions. These results suggest that the post-synthetically modified **PBFA** is a promising candidate for practical water treatment applications targeting endocrine-disrupting compounds such as BPA. Its excellent adsorption performance under mild conditions, along with its potential reusability, establishes it as an efficient material in the field of emerging adsorbents.

The post-modification of **PBFC** to obtain **PBFA** employs readily available reagents and avoids the use of highly toxic or environmentally persistent chemicals, thereby reducing the potential environmental impact during production and disposal. The synthesis also affords high yields, minimizing chemical consumption, and the hydrophobic nature of the polymer enhances its effectiveness in pollutant removal. Mild reaction conditions further reduce energy consumption and associated greenhouse gas emissions. The use of low-cost raw materials and straightforward synthesis steps makes the process economically viable for large-scale production. **PBFA** has demonstrated outstanding performance in removing organic pollutants, particularly bisphenol A, from water through hydrophobic interactions, hydrogen bonding, and strong π–π interactions. Its high adsorption capacity at near-neutral pH translates into reduced operational costs for wastewater treatment by lowering both material preparation expenses and pH adjustment requirements. The combination of high surface area and pore structure, makes **PBFA** a promising candidate for addressing challenging water purification demands.

4. Conclusion

In this study, we successfully synthesized a hypercrosslinked microporous organic polymer **PBFC** and carried out post-synthetic modification to obtain **PBFA**. Batch adsorption experiments for bisphenol-A (BPA) removal from water revealed that **PBFA** exhibits significantly enhanced adsorption performance despite having a lower surface area compared to the parent **PBFC**. This finding highlights that surface area alone is not the determining factor for efficient adsorption; rather, the presence and nature of adsorption sites play a critical role. The adsorption behaviour followed the Langmuir isotherm and pseudo-second-order kinetic model, indicating monolayer adsorption and a chemical interaction mechanism. **PBFA** achieved a maximum experimental adsorption capacity of 130 mg g^{-1}. Thermodynamic analyses confirmed the exothermic and spontaneous nature of the BPA adsorption process, with adsorption efficiency decreasing at elevated temperatures. The enhanced adsorption performance of **PBFA** is attributed to hydrophobic interactions, hydrogen bonding, and π–π stacking with BPA molecules. Moreover, **PBFA** demonstrated excellent reusability, maintaining high removal efficiency after four adsorption cycles. Overall, this work demonstrates that post-synthetic modification is an effective strategy to introduce active adsorption sites, thereby improving adsorption capacity through specific molecular interactions. **PBFA** shows strong potential as a practical and reusable adsorbent for BPA removal from aqueous environments.

Conflicts of interest

The authors declare that they have no known competing financial interests or personal relationships that could have appeared to influence the work reported in this paper.

Data availability

The data supporting this article have been included as part of the SI. The data corresponding to CHN analysis, deconvoluted XPS spectra, PXRD pattern, FESEM images, BET linear plots, and adsorption kinetic fitting curves are given in SI. See DOI: https://doi.org/10.1039/d5lp00208g.

Acknowledgements

A. R. S. and S. K. acknowledge the University of Kerala for providing research fellowships. The authors thank CLIF, University of Kerala, for instrumental support; SAIF, Indian Institute of Science Bangalore, for solid-state ^{13}C NMR analysis; and the Department of Optoelectronics, University of Kerala, for FE-SEM analysis.

References

1 A. A. Adeyi and B. A. Babalola, *Sci. Rep.*, 2019, **9**, 1–13.
2 A. Bhatnagar and I. Anastopoulos, *Chemosphere*, 2017, **168**, 885–902.
3 S. Waleed, M. Haroon, N. Ullah, M. Tuzen, I. K. Rind and A. Sarı, *Environ. Monit. Assess.*, 2025, **197**, 83.
4 O. T. Ologundudu, T. A. Msagati, O. E. Popoola and J. N. Edokpayi, *ACS Omega*, 2025, **10**, 6279–6293.
5 S. Rovani, J. J. Santos, S. N. Guilhen, P. Corio and D. A. Fungaro, *RSC Adv.*, 2020, **10**, 27706–27712.
6 M. J. F. Jasni, M. Arulkumar, P. Sathishkumar, A. R. M. Yusoff, N. A. Buang and F. L. Gu, *J. Colloid Interface Sci.*, 2017, **508**, 591–602.
7 L. Joseph, J. Heo, Y. G. Park, J. R. Flora and Y. Yoon, *Desalination*, 2011, **281**, 68–74.
8 EFSA Panel on Food Contact Materials, Enzymes and Processing Aids (CEP), C. Lambré, J. M. Barat Baviera, C. Bolognesi, A. Chesson, P. S. Cocconcelli, R. Crebelli, D. M. Gott, K. Grob, E. Lampi, M. Mengelers, A. Mortensen, G. Rivière, V. Silano, I.-L. Steffensen, C. Tlustos, L. Vernis, H. Zorn, M. Batke, M. Bignami, E. Corsini, R. FitzGerald, U. Gundert-Remy, T. Halldorsson, A. Hart, E. Ntzani, E. Scanziani, H. Schroeder, B. Ulbrich, D. Waalkens-Berendsen, D. Woelfle, Z. Al Harraq, K. Baert, M. Carfì, A. F. Castoldi, C. Croera and H. Van Loveren, *EFSA J.*, 2023, **21**, e06857.
9 R. L. Prueitt and J. E. Goodman, *Toxicol. Sci.*, 2024, **198**, 185–190.
10 J. Hao, Q. Zhang, Y. Liu, P. Chen, X. Zheng, X. Zhuang, D. Fu, H. Liu, G. Liu and W. Lv, *J. Taiwan Inst. Chem. Eng.*, 2020, **113**, 204–213.
11 B. O. Orimolade, F. A. Adekola and G. B. Adebayo, *Appl. Water Sci.*, 2018, **8**, 1–8.
12 X. Li, M. Zhou, J. Jia, J. Ma and Q. Jia, *Sep. Purif. Technol.*, 2018, **195**, 130–137.
13 C. Mo, M. Faheem, S. Aziz, S. Jian, W. Xue, T. Yuyang, G. Shuang and Z. Guangshan, *RSC Adv.*, 2020, **10**, 26335–26341.
14 Z. Yang, G. Wu, Q. Li, H. Ai, X. Yao and H. Ji, *Sep. Sci. Technol.*, 2021, **56**, 860–869.
15 Y. Liu, X. Chen, X. Jia, X. Fan, B. Zhang, A. Zhang and Q. Zhang, *Ind. Eng. Chem. Res.*, 2018, **57**, 17259–17265.
16 S. Krishnan, P. D. Raju, A. R. Sujatha and C. V. Suneesh, *J. Appl. Polym. Sci.*, 2024, **141**, e55851.
17 L. Tan and B. Tan, *Chem. Soc. Rev.*, 2017, **46**, 3322–3356.
18 Z. Liu, T. Yang, Y. Song, N. Zhao, S. Wu, Z. Ma and Z. Liu, *RSC Appl. Polym.*, 2025, **3**, 746–766.
19 D. W. Kang, M. Kang, M. Moon, H. Kim, S. Eom, J. H. Choe, W. R. Lee and C. S. Hong, *Chem. Sci.*, 2018, **9**, 6871–6877.
20 T. Ratvijitvech, R. Dawson, A. Laybourn, Y. Z. Khimyak, D. J. Adams and A. I. Cooper, *Polymer*, 2014, **55**, 321–325.
21 Y. Liang, L. Feng, X. Liu, Y. Zhao, Q. Chen, Z. Sui and N. Wang, *Chem. Eng. J.*, 2021, **404**, 127095.
22 S. Krishnan and C. V. Suneesh, *Mater. Today Commun.*, 2021, **27**, 102251.
23 S. Krishnan and C. V. Suneesh, *J. Solid State Chem.*, 2021, **299**, 122152.
24 R. M. N. Kalla, A. Varyambath, M. R. Kim and I. Kim, *Appl. Catal., A*, 2017, **538**, 9–18.
25 Y. M. Litvinov and A. M. Shestopalov, *Adv. Heterocycl. Chem.*, 2011, **103**, 175–260.
26 P. Puthiaraj, Y. R. Lee and W. S. Ahn, *Chem. Eng. J.*, 2017, **319**, 65–74.
27 X. Zhu, S. M. Mahurin, S. H. An, C. L. Do-Thanh, C. Tian, Y. Li, L. W. Gill, E. W. Hagaman, Z. Bian, J. H. Zhou and J. Hu, *Chem. Commun.*, 2014, **50**, 7933–7936.
28 X. Yang, M. Yu, Y. Zhao, C. Zhang, X. Wang and J. X. Jiang, *J. Mater. Chem. A*, 2014, **2**, 15139–15145.
29 T. J. Robshaw, A. M. James, D. B. Hammond, J. Reynolds, R. Dawson and M. D. Ogden, *J. Mater. Chem. A*, 2020, **8**, 7130–7144.
30 R. Dawson, L. A. Stevens, T. C. Drage, C. E. Snape, M. W. Smith, D. J. Adams and A. I. Cooper, *J. Am. Chem. Soc.*, 2012, **134**, 10741–10744.
31 Q. Lin, Y. Wu, X. Jiang, F. Lin, X. Liu and B. Lu, *Int. J. Biol. Macromol.*, 2019, **140**, 1–9.
32 R. Shen, X. Yan, Y. J. Guan, W. Zhu, T. Li, X. G. Liu, Y. Li and Z. G. Gu, *Polym. Chem.*, 2018, **9**, 4724–4732.
33 G. Li and Z. Wang, *J. Phys. Chem. C*, 2013, **117**, 24428–24437.
34 B. O. Orimolade, F. A. Adekola and G. B. Adebayo, *Appl. Water Sci.*, 2018, **8**, 1–8.
35 J. Wang and M. Zhang, *Int. J. Environ. Res. Public Health*, 2020, **17**, 1075.
36 J. Fan, W. Yang and A. Li, *React. Funct. Polym.*, 2011, **71**, 994–1000.
37 G. Zeng, C. Zhang, G. Huang, J. Yu, Q. Wang, J. Li, B. Xi and H. Liu, *Chemosphere*, 2006, **65**, 1490–1499.
38 M. Zbair, K. Ainassaari, A. Drif, S. Ojala, M. Bottlinger, M. Pirilä, R. L. Keiski, M. Bensitel and R. Brahmi, *Environ. Sci. Pollut. Res.*, 2018, **25**, 1869–1882.
39 A. Hu, L. Liqing, M. Zhang, Y. Liu, G. Liao and D. Wang, *J. Water Process Eng.*, 2021, **40**, 101902.
40 Y. S. Ho and G. McKay, *Process Biochem.*, 1999, **34**, 451–465.
41 W. Han, L. Luo and S. Zhang, *Int. J. Environ. Sci. Technol.*, 2012, **9**, 543–548.
42 G. Xiao, L. Fu and A. Li, *Chem. Eng. J.*, 2012, **191**, 171–176.
43 E. Baldikova, K. Pospiskova and I. Safarik, *Chem. Eng. Technol.*, 2020, **43**, 168–171.
44 N. Ayawei, A. N. Ebelegi and D. Wankasi, *J. Chem.*, 2017, **2017**, 3039817.
45 L. Liu, X. B. Luo, L. Ding and S. L. Luo, *Nanomater. Removal Pollut. Resour. Reutil.*, 2019, 83–147.
46 J. He, S. Hong, L. Zhang, F. Gan and Y. S. Ho, *Fresenius Environ. Bull.*, 2010, **19**, 2651–2656.
47 B. Ji, S. Wang, M. R. U. Silva, M. Zhang and Y. Liu, *Algal Res.*, 2021, **54**, 102198.
48 V. Yangali-Quintanilla, A. Sadmani, M. McConville, M. Kennedy and G. Amy, *Water Res.*, 2009, **43**, 2349–2362.

49 A. Waheed, N. Baig, N. Ullah and W. Falath, *J. Environ. Manage.*, 2021, **287**, 112360.
50 D. Fu, Q. Zhang, P. Chen, X. Zheng, J. Hao, P. Mo, H. Liu, G. Liu and W. Lv, *RSC Adv.*, 2021, **11**, 18308–18320.
51 X. Hu, G. Xu, H. Zhang, M. Li, Y. Tu, X. Xie and A. Li, *ACS Appl. Mater. Interfaces*, 2020, **12**, 12165–12175.
52 H. Chen, H. Xu, Y. Zhang, J. Zhou, J. He, W. Wang and L. Yang, *J. Environ. Chem. Eng.*, 2023, **11**, 111570.